$$g^{(2)}(z-z')-1=\int\frac{dk}{2\pi n}[2n_k f_k-(1-f_k)]e^{ik(z-z')}, \quad (4)$$

where $f_k=1/\sqrt{1+4/(l_\xi k)^2}$ and $n_k=1/(e^{\epsilon_k/k_BT}-1)$ is the thermal occupation of the Bogoliubov collective mode of wave number k and energy $\epsilon_k=\hbar^2k^2/(2m\sqrt{1+4/(l_\xi k)^2})$, with $l_\xi=\hbar/\sqrt{mgn}$ being the healing length. The first term in the right-hand side of Eq. (4) which accounts for thermal fluctuations is positive, whereas the second term which is the contribution of quantum (i.e., zero-temperature) fluctuations is negative [23]. Therefore, the negativity of $g^{(2)}(z-z')-1$ implies that the quantum fluctuations give a larger contribution to $g^{(2)}(z-z')-1$ than the thermal ones.

It should be emphasized, however, that the quantity we measure is $\langle\delta N^2\rangle$, and as we show below, for our large values of Δ and d it is still dominated by thermal (rather than quantum) fluctuations. This is because the contribution to $\langle\delta N^2\rangle$ of the one-body term almost cancels out the contribution of the zero-temperature two-body term. Indeed, the contribution of quantum fluctuations to $\langle\delta N^2\rangle$, calculated using Eqs. (2)–(4), is

$$\langle\delta N^2\rangle_{T=0}=\frac{\langle N\rangle}{\Delta\pi}\int_{-\infty}^{\infty}dk f_k\frac{1-\cos(k\Delta)}{k^2}e^{-k^2d^2}. \quad (5)$$

Since $f_k\propto kl_\xi$ when $kl_\xi\ll 1$, we find that for $\Delta\gg l_\xi, d$, $\langle\delta N^2\rangle_{T=0}$ scales as $nl_\xi\ln(\Delta/l_\xi)$. On the other hand, the thermal contribution given by Eq. (1), scales as $\Delta T/g$. Therefore, the quantum contribution becomes negligible as $\Delta\to\infty$, and the thermodynamic prediction of Eq. (1) is recovered [25]. For our parameters, the contribution of Eq. (5) to $\langle\delta N^2\rangle$ is shown as a dotted line in Fig. 2.

In weakly interacting gases, the atom number fluctuations take super-Poissonian values in the degenerate ideal gas and thermal quasicondensate regimes, $\langle\delta N^2\rangle/\langle N\rangle$ reaching its maximum at the quasicondensate transition where it scales as $t^{1/3}$ [3]. When t is decreased, the super-Poissonian zone is expected to merge towards the Poissonian limit and it vanishes when the gas enters the strongly interacting regime. This trend is exactly what we observe in Fig. 3(a), for $t=5.4$: at large densities, we see suppression of $\langle\delta N^2\rangle$ below the Poissonian level, but most importantly, we no longer observe super-Poissonian fluctuations at lower densities ($\langle\delta N^2\rangle/\kappa\langle N\rangle<1.3$ within the experimental resolution) [26]. Interestingly, no simple analytic theory is applicable to this crossover region, and the only reliable prediction here is the exact Yang-Yang thermodynamic solution [solid line in Fig. 3(a)].

We now describe the experimental techniques that allowed us to increase significantly $\omega_\perp$ in order to reach $t=5.4$. Keeping a reasonable heat dissipation in the wires, increasing $\omega_\perp$ requires bringing the atomic cloud closer to the chip. However, using dc microwire currents, one would observe fragmentation of the cloud due to wire imperfections and hence longitudinal roughness of the potential [27]. To circumvent this problem, we use

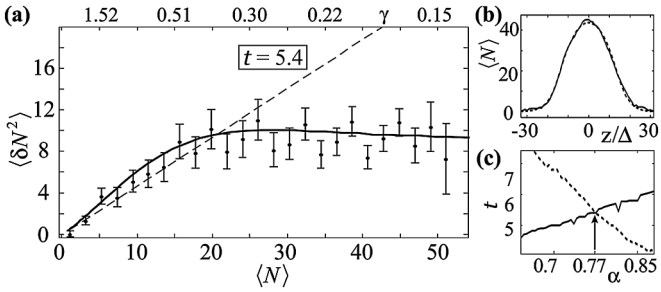

FIG. 3. (a) Variance $\langle\delta N^2\rangle$ close to the strongly interacting regime, for $t=5.4$. Different curves are as in Fig. 2, but for $\omega_\perp/2\pi=18.8$ kHz, $\omega_\parallel=7.5$ Hz, $T=40$ nK ($k_BT=0.044\hbar\omega_\perp$), and $\kappa=0.47$. (b) Average density profile (solid line) together with the Yang-Yang prediction (dashes). (c) The value of t obtained from fits to the density profile (dotted line) and atom number fluctuations (solid line) for different α (see text).

the modulation techniques developed in [28,29]. The atom chip schematic is shown in Fig. 4. The transverse confinement is realized by three wires, carrying the same ac current modulated at 200 kHz, and a longitudinal homogeneous dc magnetic field of $\sim$1.8 G realized by external coils. The modulation is fast enough so that the atoms experience the time-averaged potential, transversely harmonic. Monitoring dipole oscillations we measure $\omega_\perp/2\pi$ varying from 2 to 25 kHz, for ac current amplitude varying from 40 to 200 mA. The longitudinal confinement, with $\omega_z/2\pi$ varying from 5 to 12 Hz, is realized by wires perpendicular to the z direction, carrying dc currents of a few tens of mA. After a first rf evaporation stage in a dc trap we load 6×10^4 atoms at a few μK in the ac trap where we perform further rf evaporation at $\omega_\perp/2\pi\simeq 2$ kHz and $\omega_\parallel/2\pi\simeq 12$ Hz. Next we lower the longitudinal trapping frequency to about 7 Hz and then ramp up the transverse frequency to 18.8 kHz in 600 ms keeping the rf evaporation on during this compression. After ramping the

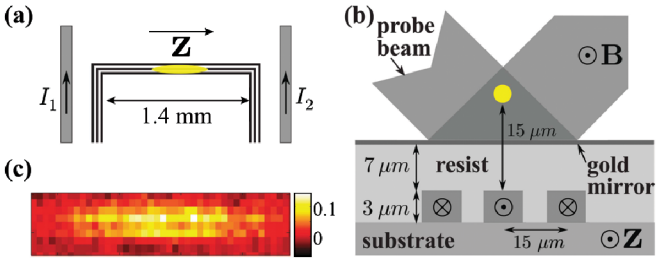

FIG. 4 (color online). (a) Wire schematic of the atom chip: three gold wires along **Z** carry an ac current and produce a tight transverse confining potential. The longitudinal confinement is realized with dc currents I_1 and I_2. (b) The wires are buried under a layer of resist, which ensures electrical insulation and surface planarization. The resist is covered with a 200 nm thick gold mirror that reflects the probe beam. The atoms are 15 μm away from the wires and see the interference pattern produced by the probe and the reflected beam. (c) Typical optical-density image of a gas of 10^3 atoms.